THE JOURNAL OF PHYSICAL CHEMISTRY C

Article

pubs.acs.org/JPCC

# Enhanced Performance of CdS/CdSe Quantum Dot Cosensitized Solar Cells via Homogeneous Distribution of Quantum Dots in $TiO_2$ Film

Jianjun Tian,[†,‡] Rui Gao,[†] Qifeng Zhang,*[,†] Shengen Zhang,*[,‡] Yanwei Li,[†] Jolin Lan,[†] Xuanhui Qu,[‡] and Guozhong Cao*[,†]

[†]Department of Materials and Engineering, University of Washington, Seattle, Washington 98195-2120, United States

[‡]Advanced Material and Technology Institute, University of Science and Technology, Beijing, 100083, China

**ABSTRACT:** The thickness and porosity of $TiO_2$ mesoporous film were optimized for better distribution of quantum dots to enhance the performance of CdS/CdSe quantum dot cosensitized solar cells. The CdS and CdSe quantum dots were prepared on $TiO_2$ mesoporous film through a successive ion layer absorption and reaction (SILAR) method and a chemical bath deposition (CBD) method, respectively. It was found that the distribution of quantum dots was inhomogeneous from the surface to the interior of the $TiO_2$ film, being mainly concentrated at the upper layer of the $TiO_2$ film. As a result, simply increasing film thickness did not make significant contribution to improving solar cell efficiency since only a small portion of quantum dots might access the interior of the film, leading to an exposure of $TiO_2$ nanoparticles in electrolyte and thus reducing the electron lifetime due to increased charge recombination rate. Our study revealed that the efficiency could reach its maximum, ~4.62%, with the $TiO_2$ film, the thickness of which was around 11 $\mu$m, and porosity was optimized by adding 12 wt % ethyl cellulose into the paste for making the $TiO_2$ film.

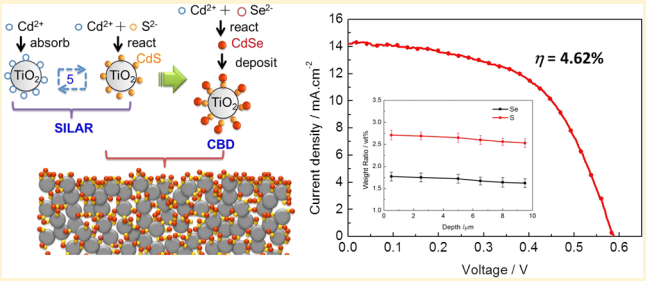


## 1. INTRODUCTION

Quantum dot sensitized solar cells (QDSCs) can be regarded as a derivative of dye-sensitized solar cells (DSCs), which have attracted worldwide scientific and technological interest since the breakthrough work done by O'Regan and Grätzel in 1991[1] for the lower cost compared to silicon-based solar cells.[2,3] Typical DSCs consist of $TiO_2$ mesoporous photoanodes, a dye sensitizer, and electrolyte.[4] A lot of work has been done to develop better dye molecules and nanostructured photoanodes over the past two decades. In DSCs, the sensitizer commonly uses organic dyes of ruthenium polypyridine complexes. To enhance light harvest in the visible light region, many efforts have been made by focusing on the development of high performance sensitizers.[5−8] It is still a challenge to obtain an ideal organic dye as sensitizer to absorb photons in the full sunlight spectra. For this reason, narrow-band gap semiconductor quantum dots (QDs), such as CdS,[9,10] CdSe,[11,12] PbS,[13] and InAs,[14] which present extraordinary optical and electrical properties over traditional organic dyes, have been paid particular attention recently. The advantages of QDs mainly involve tunable band gap upon QD sizes, high extinction coefficients, and large intrinsic dipole moment, which may facilitate charge separation in solar cells.[15,16] Theoretical photovoltaic conversion efficiency of QDSCs can reach up to 44% in view of multiple exciton generation of QDs. Such an efficiency is much higher than the 31% for semiconductor solar cells according to the Schockley-Queisser limit.[17]

Among various materials that are used for QDSCs, CdS, and CdSe are attractive owing to their high potential in light harvest in the visible-light region.[16,18] CdSe has a band gap of 1.7 eV and may therefore absorb photons with wavelengths shorter than 700 nm. The research of Wang et al.[19] showed that CdSe-sensitized $TiO_2$ solar cells incorporating lights scattering layers presented an unprecedented power conversion efficiency of 5.21%. However, it was found that CdSe was difficult to deposit directly on oxides, such as $TiO_2$ and ZnO. For this reason, modification of oxide with CdS has been usually adopted to improve the adsorption of CdSe.[20,21] The other reason that CdS has been used is to form CdS/CdSe cosensitization to broaden the optical absorption of the solar cells. So far, CdS/CdSe cosensitized QDSCs have reached power conversion efficiency (PCE) higher than 4%.[22,23] Most recently, Santra and Kamat reported that QDSC with Mn-doped CdS/CdSe achieved power conversion efficiency of 5.4%.[24]

In a typical process for the fabrication of QDSC photoelectrode, QDs can be introduced via two approaches: (a) in situ growth directly from the precursor solutions, and (b) adsorption of presynthesized QDs with or without bifunctional

**Received:** June 15, 2012
**Revised:** August 12, 2012
**Published:** August 13, 2012

   dx.doi.org/10.1021/jp3058838 | J. Phys. Chem. C 2012, 116, 18655−18662

linker. However, the QDSCs produced with the latter approach have reported relatively low conversion efficiency, largely due to the difficulty in achieving sufficient coverage of QDs.[11] The former, i.e., in situ growth of QDs, includes chemical bath deposition (CBD)[25] and successive ionic layer absorption and reaction (SILAR),[26,27] and have shown better performance than the latter when being adopted to assemble QDSCs. In the case of solar cells cosensitized by CdS/CdSe QDs, the CdS QD layer serves as both a seeding layer to facilitate the subsequent CdSe QD growth and an energy barrier layer to reduce the back charge recombination between the electrons in oxide and the holes in electrolyte.[28−30] Figure 1 shows the cell structure

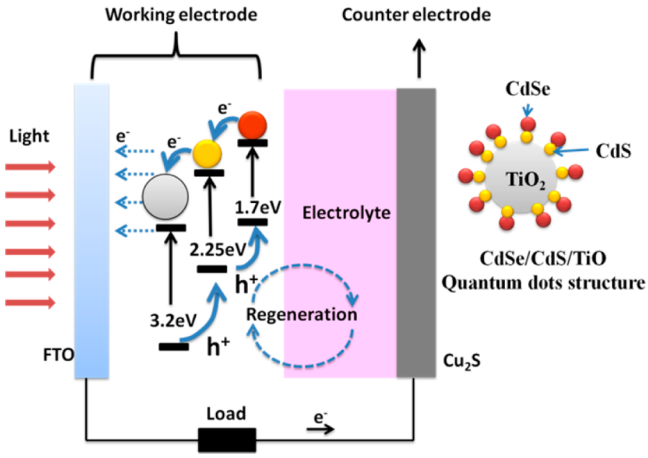


**Figure 1.** Sketch of the photoelectrical conversion structure of a QDSC.

of a CdS/CdSe cosensitized QD solar cell, which consists of a $TiO_2$ mesoporous film (photoanodes), CdS/CdSe QDs (sensitizer), polysulfide electrolyte, and $Cu_2S$ counter electrode. During operation, photons are captured by QDs, yielding electron−hole pairs that are rapidly separated to electrons and holes at the interface between the nanocrystalline $TiO_2$ and the QDs. The electrons inject into the oxide film and the holes are released by redox couples in the liquid polysulfide electrolyte.

From the working mechanism of QDSCs mentioned above, we can see that the amount of adsorbed QDs, electron transport, and lifetime are the key factors affecting the performance of QDSCs. These factors have a close relationship with the structure of mesoporous anode film. Compared with traditional dye molecules used in DSCs, QDs usually have bigger particle size, and as a result, are hard to enter into the deep pores of the anode film. This scenario not only decreases the QDs load, but also results in a nonuniform distribution of QDs from the surface to the bottom of the mesoporous film. Therefore, the appropriate mesoporous anode films for the QDSCs are worth investigating so as to improve the distribution of QDs and thus enhance the performance of QDSCs. In this paper, the relationship between QDs distribution, particle size, electron lifetime, and the film thickness was studied. It was found that $TiO_2$ mesoporous films for QDSCs could be optimized by adjusting the film thickness and the content of ethyl cellulose (EC), which is one of components determining the viscosity of paste for making film, resulting in achieving power conversion efficiency up to 4.62%.

## 2. EXPERIMENTAL PROCEDURES

**2.1. Preparation of Mesoporous $TiO_2$ Films.** $TiO_2$ pastes were prepared by mixing $TiO_2$ nanoparticles (Degussa P25), EC, and $\alpha$ -terpineol following a previously reported procedure.[31] The paste was then coated on a fluorine-doped tin oxide (FTO) glass substrate via the doctor blading method to get mesoporous films with different thicknesses. The as-received $TiO_2$ films underwent a sintering process in air as follows: 125 °C for 30 min and at 500 °C for 30 min at heating speed of 5 °C/min. The area of the $TiO_2$ films was approximately 0.36 $cm^2$ (0.6 cm ×0.6 cm square).

**2.2. Preparation of CdS/CdSe Cosensitized Photoelectrodes.** For the growth of CdS QDs, first, the $TiO_2$ film was immersed into a 0.1 M cadmium nitrate ($Cd(NO_3)_2$) methanol solution for 1 min. Successively, the film was dipped into a 0.1 M sodium sulfide ($Na_2S$) methanol solution for another 1 min to allow $S^{2-}$ to react with the preadsorbed $Cd^{2+}$, leading to the formation of CdS. This procedure was called one SILAR cycle. In total, five cycles were employed to obtain a

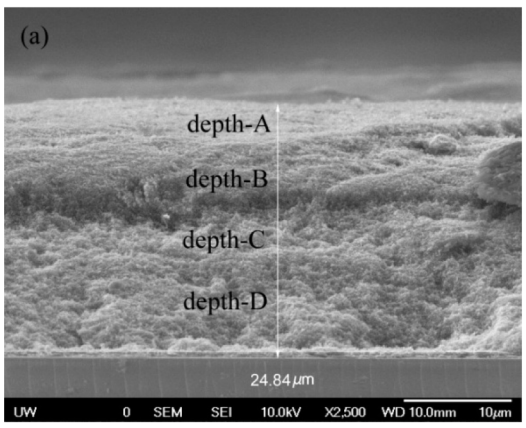


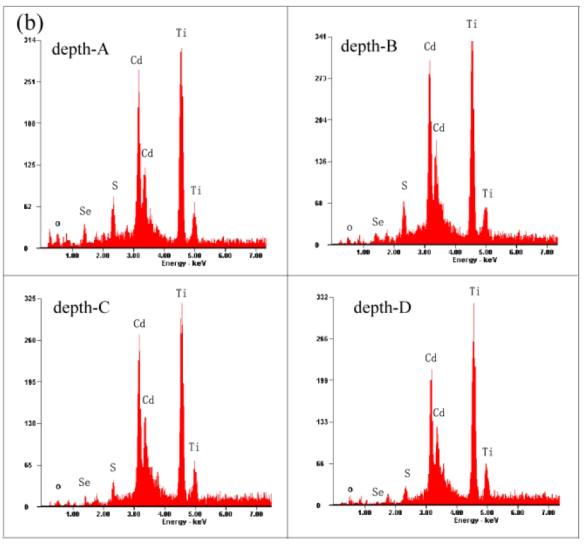


**Figure 2.** (a) SEM image of the film transverse and (b) EDX images corresponding to different depths of the film.


dx.doi.org/10.1021/jp3058838 | J. Phys. Chem. C 2012, 116, 18655−18662

Table 1. Weight Ratio of the Elements Measured by EDX in the Different Depths of the Film[a]

| depth | S, wt% | Se, wt% | Cd, wt% | Ti, wt% | O, wt% |
|---|---|---|---|---|---|
| A | 2.94(±0.11) | 1.72(±0.09) | 38.14(±0.32) | 55.62(±0.51) | 1.58(±0.10) |
| B | 2.45(±0.10) | 1.32(±0.10) | 36.41(±0.37) | 57.59(±0.57) | 2.23(±0.09) |
| C | 2.18(±0.10) | 0.86(±0.08) | 35.23(±0.29) | 59.10(±0.63) | 2.62(±0.08) |
| D | 1.30(±0.07) | 0.66(±0.06) | 33.52(±0.34) | 61.91(±0.61) | 2.62(±0.08) |

[a]The standard deviation of the properties is based on the data of three times measured.

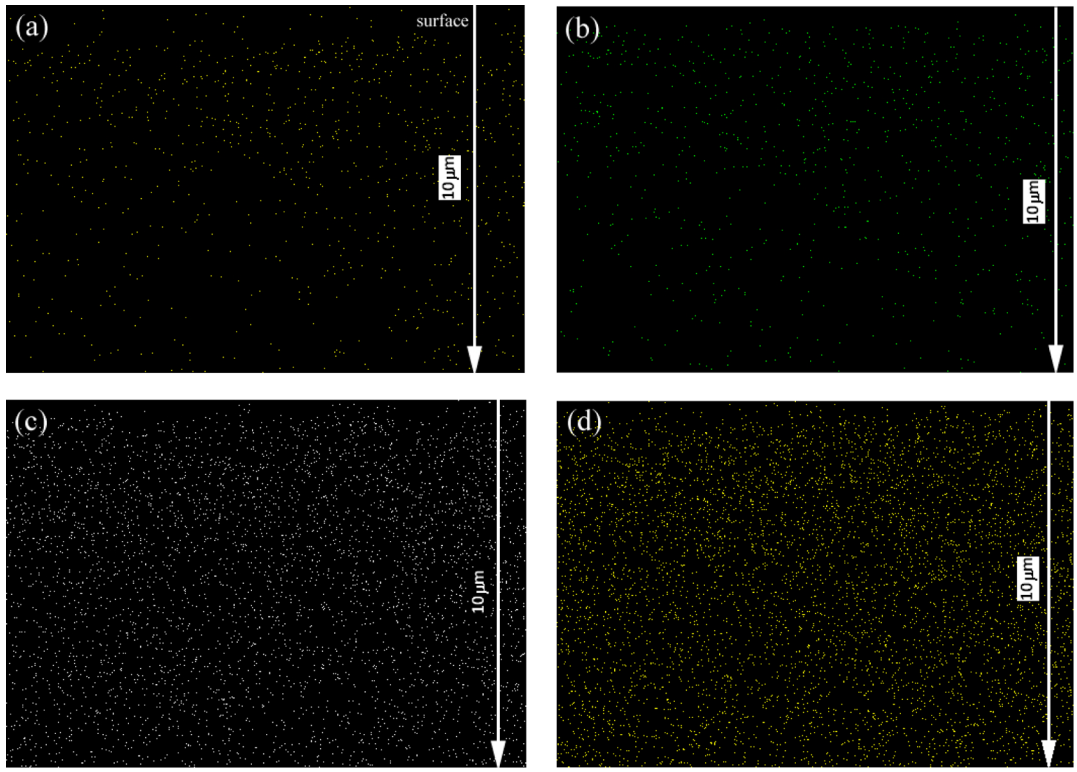


Figure 3. Element distribution maps of (a) Se, (b) S, (c) Cd, and (d) Ti.

suitable amount of CdS on the $TiO_2$ film. In a sequent step, CdSe was deposited on the CdS-coated $TiO_2$ film through a CBD method. Briefly, 0.1 M sodium selenosulphate ($Na_2SeSO_3$) aqueous, 0.1 M cadmium acetate $Cd(CH_2COO)_2$ aqueous solution, and 0.2 M trisodium salt of nitrilotriacetic acid ($N(CH_2COONa)_3$) solution were mixed together with a volume ratio of 1:1:1. Then the CdS-coated $TiO_2$ film was vertically immersed into the solution for the deposition of a CdSe layer under dark conditions at 24 °C for 3 h. After the deposition of CdSe, a ZnS passivation layer was deposited by two SILAR cycles while being soaked in an aqueous solution containing 0.1 M zinc nitrate and 0.1 M sodium sulfide, which act as $Zn^{2+}$ and $S^{2-}$ sources, respectively.

**2.3. Electrolyte and Counter Electrode.** The electrolyte employed in this study was composed of 1 M S and 1 M $Na_2S$ in deionized water. The counter electrode was a $Cu_2S$ film fabricated on brass foil. The preparation of the $Cu_2S$ electrode can be described as follows: brass foil was immersed into 37% HCl at 70 °C for 5 min, then rinsed with water and dried in air. After that, the etched brass foil was dipped into 1 M S and 1 M $Na_2S$ aqueous solution, resulting in a black $Cu_2S$ layer forming on the foil.

**2.4. Characterization of Materials and QDSCs.** The morphology was characterized by a scanning electron microscope (SEM, JSM-7000). Energy dispersion X-ray (EDX) was used to analyze the element contents and distribution. The photovoltaic properties were measured using an HP 4155A programmable semiconductor parameter analyzer under AM 1.5 simulated sunlight with the power density of 100 mW/cm$^2$. A thermal scientific UV−vis−NIR spectrum meter was used to study the samples' light absorption properties. Electrochemical impedance spectra (EIS) were measured in the dark by applying an oscillation potential of −0.6 V from $10^{-1}$ to $10^6$ Hz.

## 3. RESULTS AND DISCUSSION

Figure 2 Shows the SEM and EDX images in the different depth sections of the photoanode film with the thickness of 25 $\mu$m. The element weight ratios are listed in Table 1. It can be seen that the energy dispersion peaks of Se and S drop gradually from the surface to the bottom of the film. On the basis of EDX calculation, Se and S contents decrease from ~1.72 wt % to ~0.66 wt %, and ~2.94 wt % to ~1.30 wt %, respectively. Figure 3 shows the EDX mapping images of Se, S, Cd, and Ti from the surface to a depth of 10 $\mu$m along the transverse of the film. We can see that Se and S concentrate on the upper section and evidently decrease with increase of depth in the film. Therefore, QDs (CdSe and CdS) distribute inhomogeneously from the surface to the bottom of the film. There are several possible explanations: (1) the residual liquid when the substrate was withdrawn from the precursor solution


dx.doi.org/10.1021/jp3058838 | J. Phys. Chem. C 2012, 116, 18655−18662

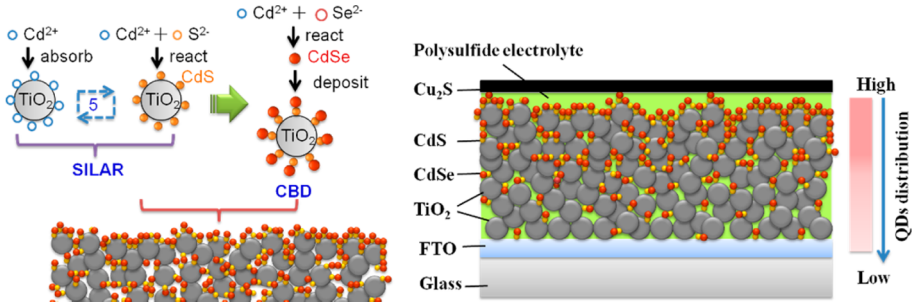


**Figure 4.** Sketch of the formation and distribution of CdS/CdSe QDs on the mesoporous $TiO_2$ substrate: (a) formation process of QDs; (b) solar cell structure and distribution of QDs.

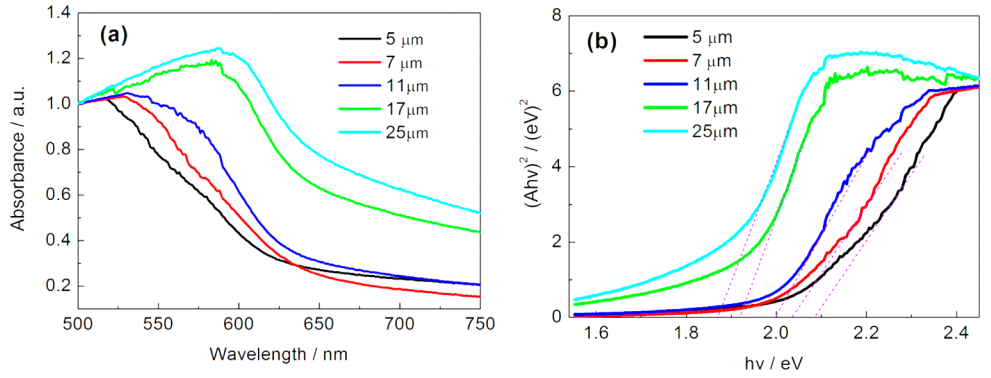


**Figure 5.** (a) UV–vis spectra and (b) $(Ahv)^2$ vs $h\nu$ curves of the film samples with different thicknesses.

(effectively a dip-coating process), (2) the existence of air bubbles trapped insides the porous film preventing the complete filling of precursor solution, (3) the incomplete removal of liquid from the SILAR process, and (4) fast formation of QDs in the upper section and prevention of precursor solution from entering into deep pores. For example, during the SILAR process, the film was first immersed in $Cd^{2+}$ solution, and then $Cd^{2+}$ filled into all the pores of the film. When the film was dipped in $S^{2-}$ solution, CdS particles were formed quickly and blocked some pores in the upper section of the film, which prevented the $S^{2-}$ solution from infusing into the deep pores. So $Cd^{2+}$ in the deep pores cannot completely react with $S^{2-}$. This demonstrates that the Cd element distributes uniformly from the surface to the bottom of the film (as shown in Figure 3c) and the amount of Cd is excessive in comparison with the sum of Se and S (as shown in Table 1). So CdS QDs mainly concentrate on the upper section of the film. Additionally, the formation process of CdS/CdSe QDs, which is mainly based on ion diffusion, also affects the distribution of QDs in the film. Figure 4 shows a sketch of the formation process and distribution of CdS/CdSe QDs on a $TiO_2$ mesoporous film. The CdS QDs were first synthesized by SILAR on the surface of $TiO_2$ nanoparticles, which is termed $TiO_2$/CdS in this paper. After that, CdSe QDs were gradually deposited to combine with CdS QDs to form a structure of $TiO_2$/CdS/CdSe. Compared with organic dyes, CdS and CdSe QDs have bigger particle size. Therefore, QDs are likely to be able to block the upper pores of the film and thus prevent the formation of CdSe QDs in the interior of the $TiO_2$ film. As a result, as shown in Figure 4b, CdSe and CdS particles mainly focus on the upper section of the film. In this paper, we do not have any idea about ZnS, because ZnS is only used as a passivation layer of CdSe to enhance the performance of a photoelectrode.[20]

Figure 5a shows the UV–vis absorption spectra of CdS/CdSe/$TiO_2$ films with different thickness. In order to remove the light scattering effect of $TiO_2$ films, the spectra curves were obtained by deducting the absorbance of $TiO_2$ films with different thickness. It is found that the absorption of the films increases with the increasing film thickness, indicating that the amount of QDs increases accordingly. The shift of absorption edges from the short to long wavelength with the increase of the film thickness suggests that CdSe QDs get larger with an increasing film thickness. The size of CdSe QD can be estimated using the UV–visible absorption spectrum.[12,20,32] It is not the intention of this paper to discuss the size of CdS, because the CdS layer serves as the seed layer to enhance the CdSe growth rate and is surrounded by CdSe.[22,23] However, it is known that the optical band gap ($E_g$) for direct interband transitions and the absorption coefficient ($A$) near the absorption edge has a relationship that complied with the following equation (eq 1):[33−35]

$$(Ah\nu)^2 = c(h\nu - E_g) \tag{1}$$

where the optical band gap for the absorption edge can be obtained by extrapolating the linear portion of the plot $(Ahv)^2$-$hv$ to $A = 0$. $E_g$ of CdSe can be obtained from Figure 5b. The size of the CdSe QDs can be estimated using eq 2:[12,32]

$$\Delta E = E_1 - E_g = \frac{h^2}{8r^2}\left(\frac{1}{m_e} + \frac{1}{m_h}\right) \tag{2}$$

where $\Delta E$ is the band gap shift, $r$ is the QD radius, $E_1$ is the band gap of CdSe, $E_g$ is the band gap of the bulk materials (1.74 eV for CdSe bulk material), and $m_e$ and $m_h$ are the effective masses of electron and hole, respectively. For CdSe material, the $m_e = 0.13m_0$ and $m_h = 0.44m_0$ ($m_0 = 9.11 \times 10^{-31}$ kg). The results are shown in Figure 6. It can be seen that the size of the


dx.doi.org/10.1021/jp3058838 | J. Phys. Chem. C 2012, 116, 18655−18662

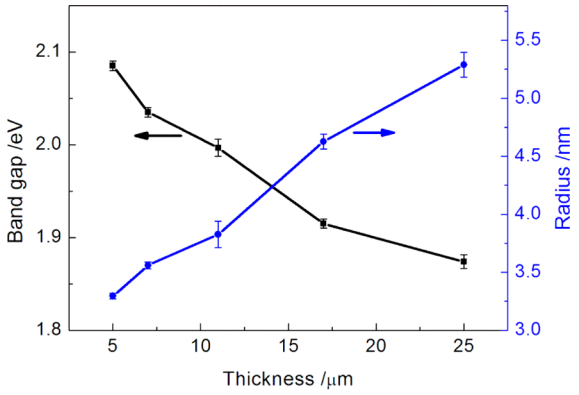


**Figure 6.** Band gaps (left) and particle sizes (right) of the CdSe QDs as functions of film thickness.

CdSe QDs increases slowly and remains small (≤3.8 nm) in the case of film thickness less than 11 $\mu$m. However, the size evidently increases when the films are more than 11 $\mu$m thick. The particle size almost increases by 60% when the film thickness increases from 5 to 25 $\mu$m. This result is against our common sense. The formation of CdSe QDs can be regarded as homogeneous nucleation during the CBD process. So the size distribution of the nanoparticles is dependent on the subsequent growth process of the nuclei. On the basis of the above results of distribution of CdSe, the precursor solution concentration decreases gradually from the surface to the bottom of the film. It was reported[36] that a high concentration precursor solution has a large number of initial nuclei formed in the nucleation stage, which results in a larger number of nanoparticles with smaller size. So CdSe in the upper section of the film has more and smaller particle sizes than those of CdSe in bottom of the film. In view of the QD distribution concentrating at the upper layer of the $TiO_2$ film, it can be deduced that an increase in the amount of QDs cannot effectively improve the photoelectricity conversion efficiency of QDSCs.

$TiO_2$/CdS/CdSe photoelectrode films with different thicknesses were used to assemble solar cells. Figure 7 shows the photocurrent−voltage ($J$−$V$) curves for the solar cells measured under the illumination of 1 sun (AM 1.5, 100 mW cm$^{-2}$). The performance parameters of the solar cells, including open circuit potential ($V_{oc}$), short circuit current ($J_{sc}$), fill factor (FF) and power conversion efficiency ($\eta$), are listed in Table 2. It can be seen that $J_{sc}$ increases with the increase of film thickness

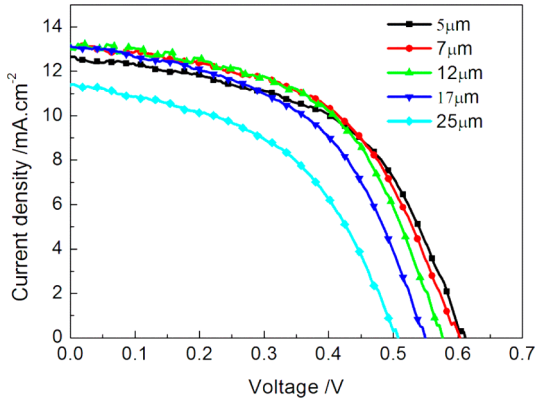


**Figure 7.** $J$−$V$ curves of the samples with different thicknesses.

from 5 to 17 $\mu$m. The increase of $J_{sc}$ is mainly caused by the increase of CdSe amount for more optical absorption. However, while the film thickness further increases, for example, reaches 25 $\mu$m, the electron transport path becomes longer than the diffusion length of electrons in $TiO_2$ nanocrystalline film, leading to increased recombination between the electrons and holes. As a result, $J_{sc}$ turns to decrease evidently. From the results shown in Table 2, we can also see that $V_{oc}$ decreases continuously as increasing film thickness. This further evidences the existence of charge recombination, which is related to the electron diffusion. A thicker film results in longer electron diffusion distance and therefore higher recombination rate. This eventually results in lower open-circuit voltage. The efficiency $\eta$ can be calculated using eq 3. In our study, the highest efficiency, ~4.16%, was obtained when the film was 7 $\mu$m in thickness. This can be explained by the inhomogeneous distribution of QDs in the $TiO_2$ nanocrystalline film, which mainly concentrates at the top layer in the region of 7 $\mu$m.

$$\eta(\%) = [(\mathrm{FF} \times V_{oc} \times J_{sc})/V_{max} \times J_{max}] \times 100 \quad (3)$$

To better understand the relationship between the performance of QDSCs and the thickness of photoanode film, the charge transport property was measured using EIS. Figure 8 shows the impedance spectra of the QDSCs measured under forward bias (−0.6 V) under dark conditions. In Figure 8a, the two semicircles correspond to the electron injection at the counter electrode/electrolyte interface and transport in the electrolyte at high frequencies ($R_1$), and the electron transfer at the $TiO_2$/QDs/electrolyte interface and transport in the $TiO_2$ film ($R_2$), respectively.[37] The charge transport properties of QDSCs are listed in Table 3. It can be seen that $R_2$ decreases with increase of film thickness, especially, drops evidently when the thickness is above 11 $\mu$m. The decrease of $R_2$ is mainly attributed to the increase of the contact of $TiO_2$ to electrolyte, which drains the electrons in the $TiO_2$ and facilitates the electron injection from the FTO film.[38] The electron lifetime ($\tau_n$) calculated according to Figure 8b ($1/2\pi f_{max}$)[39] are shown in Figure 8c and Table 3. It indicates that $\tau_n$ can remain high value, ~10 ms, when the photoelectrode film is thinner than 11 $\mu$m. However, the electron lifetime drops to ~4 ms when the film is thicker than 11 $\mu$m.

According to the EIS results, the most appropriate thickness for photoanode film should be around 11 $\mu$m, which gives the longest electron lifetime. However, in our study, the efficiency obtained for the film with 7 $\mu$m thickness is higher than that of the film with 11 $\mu$m thickness, as shown in Table 2. This can be explained by the distribution of QDs in the nanocrystalline film, i.e., incremental amount of QDs in the films thicker than 7 $\mu$m mainly concentrates at the upper section of the film. These QDs may cause more optical absorption; however, they do not contribute to solar cell efficiency in view of the loss of electrons during transport due to recombination.

According to the discussion above, we can know that, to further enhance the performance of QDSCs, the pores of $TiO_2$ film should be increased so that the CdSe QDs would be able to grow into the deep-seated pores of the film during the CBD process. To this end, we increased the content of the additive of EC in the paste so as to enhance the porosity of the $TiO_2$ films. Figure 9 shows $J$−$V$ curves of QDSCs with photoanode films prepared with pastes different in EC content. Detailed results of the samples are shown in Table 4. It can be seen that the efficiency of QDSCs increases from 4.09% to 4.62% when the


dx.doi.org/10.1021/jp3058838 | J. Phys. Chem. C 2012, 116, 18655−18662

**Table 2. Properties of the Samples with Different Thicknesses[a]**

| samples | thickness, $\mu$m | $V_{oc}$, V | $J_{sc}$, mA·cm$^{-2}$ | FF | $\eta$, % |
|---|---|---|---|---|---|
| T1 | 5 | 0.61(±0.01) | 12.66(±0.25) | 0.53(±0.01) | 4.06(±0.09) |
| T2 | 7 | 0.60(±0.01) | 13.05(±0.22) | 0.53(±0.01) | 4.16(±0.11) |
| T3 | 11 | 0.58(±0.01) | 13.04(±0.21) | 0.54(±0.01) | 4.09(±0.12) |
| T4 | 17 | 0.55(±0.01) | 13.11(±0.18) | 0.51(±0.01) | 3.66(±0.10) |
| T5 | 25 | 0.51(±0.01) | 11.39(±0.27) | 0.49(±0.01) | 2.79(±0.11) |

[a]The standard deviation of the properties is based on the data of three cells.

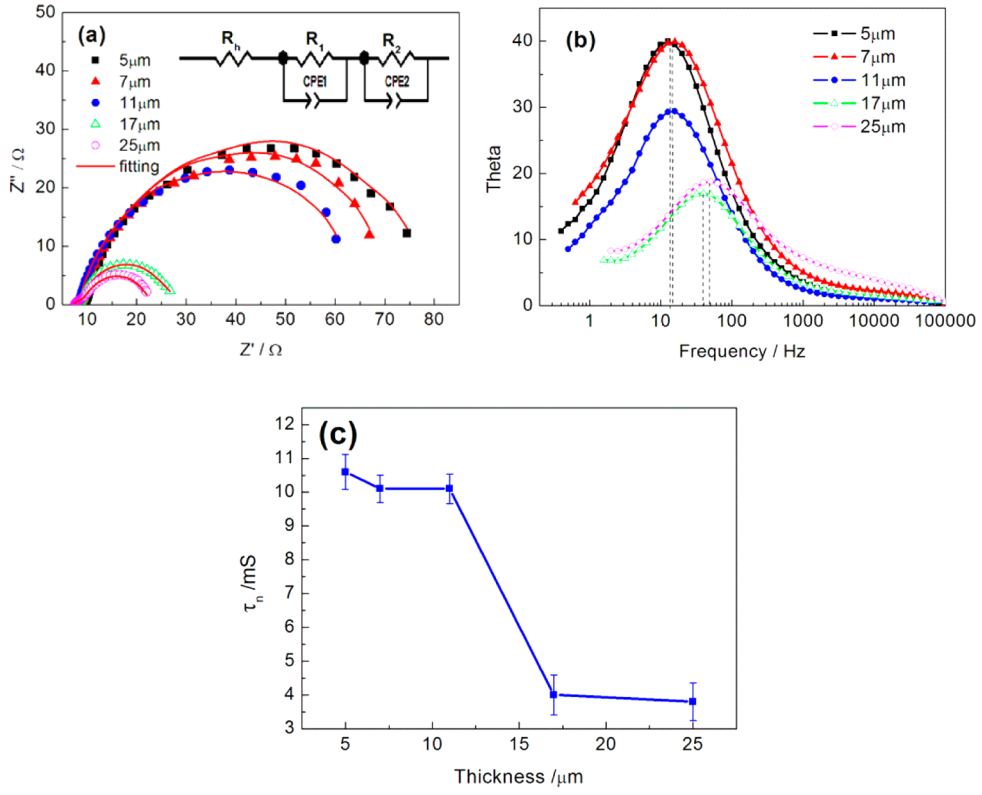


**Figure 8.** (a) Nyquist plots, (b) Bode plots and (c) electron lifetimes of QDSCs with various layer thicknesses in the dark at an applied forward bias of −0.6 V.

**Table 3. EIS Results of the Layer with Different Thicknesses: Charge Transfer Resistance and Electron Lifetime[a]**

| samples | thickness, $\mu$m | $R_1$, Ω | $R_2$, Ω | $\tau_n$, ms |
|---|---|---|---|---|
| T1 | 5 | 0.6 (±0.37) | 71.9 (±9.52) | 10.6 (±0.52) |
| T2 | 7 | 1.3 (±0.55) | 66.9 (±7.02) | 10.1 (±0.41) |
| T3 | 11 | 1.0 (±0.69) | 56.6 (±8.23) | 10.1 (±0.44) |
| T4 | 17 | 1.1 (±0.46) | 18.3 (±7.13) | 4.0 (±0.59) |
| T5 | 25 | 2.8 (±0.91) | 12.9 (±5.83) | 3.8 (±0.56) |

[a]The standard deviation of the properties is based on the data of three cells.

EC content increases from initial 9 wt % to 12 wt %. When the EC content is further increased, the solar cell efficiency, however, decreases, because of the too big pores of the $TiO_2$ film giving rise to low internal surface area and therefore less CdSe QD adsorption.

Figure 10 shows element distribution along the transverse of an 11-um-thick film produced with the paste containing 12 wt % EC. Comparing with Figure 4, the distribution of Se and S elements in the interior of $TiO_2$ film is obviously improved due to the increase of film's porosity. In other words, even though the film thickness is increased from 7 to 11 $\mu$m, the distribution

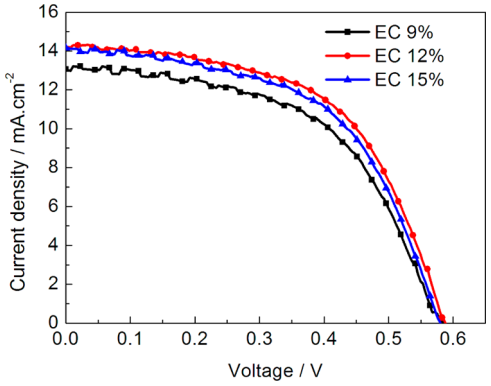


**Figure 9.** $J$–$V$ curves of the samples with different EC contents.

of QDs is still quite uniform from the upper layer to the bottom of the film. This would allow using a thicker film to achieve more QD adsorption so as to increase solar cell efficiency. Shown in Figure 11 are the EIS of solar cells with 11-um-thick photoanode films which are, however, different in porosity. It can be seen that an increase in $R_2$ for the $TiO_2$ film in which porosity is increased through using more EC implies that the


dx.doi.org/10.1021/jp3058838 | J. Phys. Chem. C 2012, 116, 18655−18662

**Table 4. Properties of the Samples with Different EC Contents and Thickness Layers[a]**

| samples | EC content, wt% | thickness, $\mu$m | $V_{oc}$, V | $J_{sc}$, mA/cm$^2$ | FF | $\eta$, % |
|---|---|---|---|---|---|---|
| C1 | 9 | 10.9 | 0.58(±0.01) | 13.04(±0.21) | 0.54(±0.01) | 4.09(±0.12) |
| C2 | 12 | 10.3 | 0.59(±0.01) | 14.23(±0.27) | 0.55(±0.01) | 4.62(±0.14) |
| C3 | 15 | 10.1 | 0.58(±0.01) | 14.16(±0.26) | 0.54(±0.01) | 4.47(±0.13) |

[a]The standard deviation of the properties is based on the data of three cells.

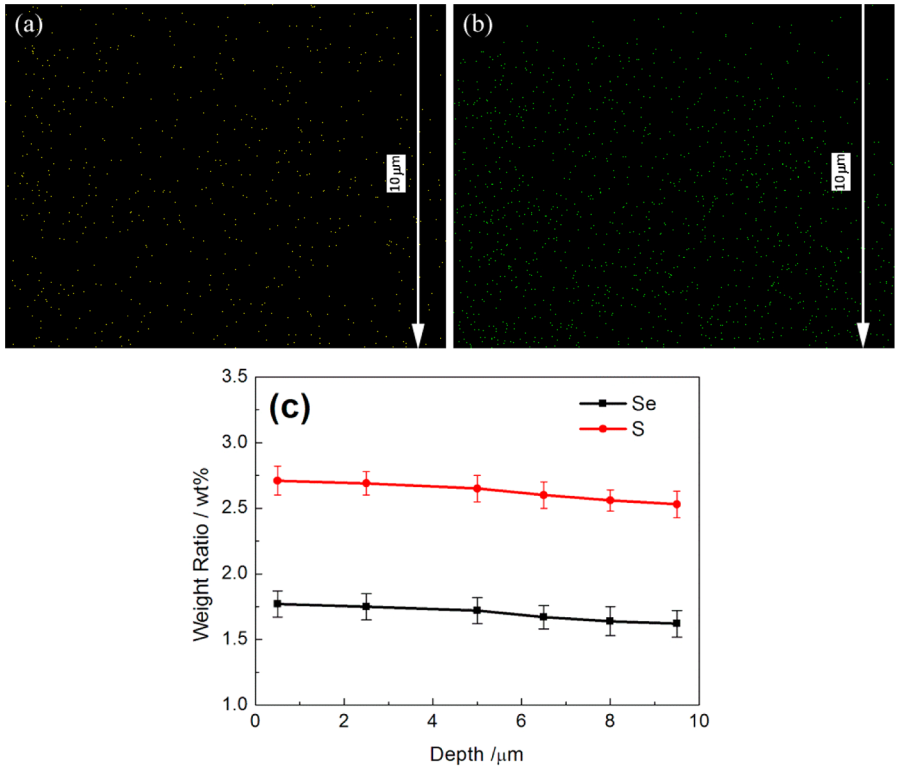


**Figure 10.** (a) Se and (b) S distribution maps and (c) elements content curves from surface to bottom in the sample with 12% EC.

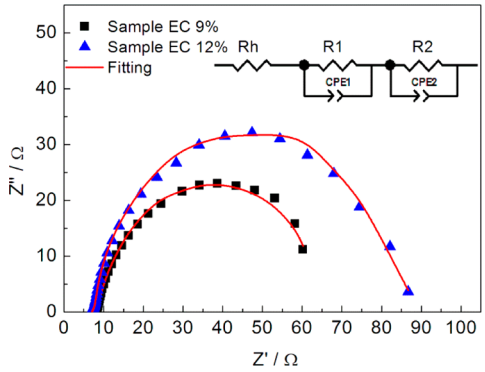


**Figure 11.** Nyquist plots of EIS spectra measured in the dark at an applied forward bias of −0.6 V.

contact area of $TiO_2$ nanoparticles with electrolyte has been reduced, leading to decreased electron recombination.

## 4. CONCLUSIONS

Our study reveals that it is difficult to achieve homogeneous distribution of QDs in nanocrystalline film from the surface to interior. The main portion of QDs concentrates at the upper layer of the film, resulting in the direct exposure of $TiO_2$ film in electrolyte and therefore serious recombination between the electrons in $TiO_2$ and the holes in electrolyte. Increasing the porosity of $TiO_2$ films by adding EC in paste has shown to significantly improve the distribution of QDs. The highest power conversion efficiency of 4.64% was received after an optimization of the film thickness and porosity.

## AUTHOR INFORMATION

### Corresponding Author

*E-mail: gzcao@u.washington.edu.

### Notes

The authors declare no competing financial interest.

## ACKNOWLEDGMENTS

The fabrication and characterization of QDSCs were supported by the U.S. Department of Energy, Office of Basic Energy Sciences, Division of Materials Sciences, under Award no. DE-FG02-07ER46467 (Q.F.Z.). This work is also supported in part by National Science Foundation (DMR 1035196), the University of Washington TGIF grant, the Royalty Research Fund (RRF) from the Office of Research at University of Washington, National Science Foundation of China (51004011 and 51174247), the Fundamental Research Funds for the Central Universities (FRF-TP-12-153A), and the Research Fund for the Doctoral Program of Higher Education (20090006120012). JJT would also like to acknowledge the fellowship from China Scholar-ship Council.

## REFERENCES


(1) Oregan, B.; Gratzel, M. *Nature* **1991**, *353*, 737−740.
(2) Barbe, C. J.; Arendse, F.; Comte, P.; Jirousek, M.; Lenzmann, F.; Shklover, V.; Gratzel, M. *J. Am. Ceram. Soc.* **1997**, *80*, 3157−3171.
(3) Yella, A.; Lee, H. W.; Tsao, H. N.; Yi, C. Y.; Chandiran, A. K.; Nazeeruddin, M. K.; Diau, E. W. G.; Yeh, C. Y.; Zakeeruddin, S. M.; Gratzel, M. *Science* **2011**, *334*, 629−634.
(4) Zhang, Q. F.; Cao, G. Z. *Nano Today* **2011**, *6*, 91−109.
(5) Bessho, T.; Yoneda, E.; Yum, J. H.; Guglielmi, M.; Tavernelli, I.; Imai, H.; Rothlisberger, U.; Nazeeruddin, M. K.; Gratzel, M. *J. Am. Chem. Soc.* **2009**, *131*, 5930−5934.
(6) Bomben, P. G.; Robson, K. C. D.; Sedach, P. A.; Berlinguette, C. P. *Inorg. Chem.* **2009**, *48*, 9631−9643.
(7) Johansson, P. G.; Rowley, J. G.; Taheri, A.; Meyer, G. J. *Langmuir* **2011**, *27*, 14522−14531.
(8) Zhao, H. C.; Harney, J. P.; Huang, Y. T.; Yum, J. H.; Nazeeruddin, M. K.; Gratzel, M.; Tsai, M. K.; Rochford, J. *Inorg. Chem.* **2012**, *51*, 1−3.
(9) Kim, J.; Choi, H.; Nahm, C.; Moon, J.; Kim, C.; Nam, S.; Jung, D.-R.; Park, B. *J. Power Sources* **2011**, *196*, 10526−10531.
(10) Panigrahi, S.; Basak, D. *J. Colloid Interface Sci.* **2011**, *364*, 10−17.
(11) Robel, I.; Subramanian, V.; Kuno, M.; Kamat, P. V. *J. Am. Chem. Soc.* **2006**, *128*, 2385−2393.
(12) Shen, Q.; Kobayashi, J.; Diguna, L. J.; Toyoda, T. *J. Appl. Phys.* **2008**, *103*, 084304.
(13) Plass, R.; Pelet, S.; Krueger, J.; Gratzel, M.; Bach, U. *J. Phys. Chem. B* **2002**, *106*, 7578−7580.
(14) Yu, P.; Zhu, K.; Norman, A. G.; Ferrere, S.; Frank, A. J.; Nozik, A. J. *J.Phys. Chem. B* **2006**, *110*, 25451−25454.
(15) Gonzalez-Pedro, V.; Xu, X.; Mora-Sero, I.; Bisquert, J. *Acs Nano* **2010**, *4*, 5783−5790.
(16) Zhu, G.; Pan, L.; Xu, T.; Sun, Z. *Acs Appl. Mater. Inter.* **2011**, *3*, 3146−3151.
(17) Hanna, M. C.; Nozik, A. J. *J. Appl. Phys.* **2006**, *100*, 074510.
(18) Lee, Y. H.; Im, S. H.; Chang, J. A.; Lee, J. H.; Seok, S. I. *Org. Electron.* **2012**, *13*, 975−979.
(19) Hossain, Md. Anower; Jennings, James Robert; Shen Chao; Pan, Jia Hong; Yu, Koh Zhen; Nripan, Mathews; Qing., W. *J. Mater. Chem.* **2012**, *22*, 16235−16242.
(20) Chong, L.-W.; Chien, H.-T.; Lee, Y.-L. *J. Power Sources* **2010**, *195*, 5109−5113.
(21) Zarazua, I.; De la Rosa, E.; Lopez-Luke, T.; Reyes-Gomez, J.; Ruiz, S.; Angeles Chavez, C.; Zhang, J. Z. *J. Phys. Chem. C* **2011**, *115*, 23209−23220.
(22) Yu, X.-Y.; Liao, J.-Y.; Qiu, K.-Q.; Kuang, D.-B.; Su, C.-Y. *Acs Nano* **2011**, *5*, 9494−9500.
(23) Zhang, Q.; Guo, X.; Huang, X.; Huang, S.; Li, D.; Luo, Y.; Shen, Q.; Toyoda, T.; Meng, Q. *Phys. Chem. Chem. Phys.* **2011**, *13*, 4659−4667.
(24) Santra, P. K.; Kamat, P. V. *J. Am. Chem. Soc.* **2012**, *134*, 2508−2511.
(25) Huang, X.; Huang, S.; Zhang, Q.; Guo, X.; Li, D.; Luo, Y.; Shen, Q.; Toyoda, T.; Meng, Q. *Chem. Commun.* **2011**, *47*, 2664−2666.
(26) Lee, Y. L.; Lo, Y. S. *Adv. Funct. Mater.* **2009**, *19*, 604−609.
(27) Yang, Z.; Zhang, Q.; Xi, J.; Park, K.; Xu, X.; Liang, Z.; Cao, G. *Sci. Adv. Mater.* 2012, In press.
(28) Lee, H.; Wang, M.; Chen, P.; Gamelin, D. R.; Zakeeruddin, S. M.; Graetzel, M.; Nazeeruddin, M. K. *Nano Lett.* **2009**, *9*, 4221−4227.
(29) Toyoda, T.; Oshikane, K.; Li, D. M.; Luo, Y. H.; Meng, Q. B.; Shen, Q. *J. Appl. Phys.* **2010**, *108*, 114304.
(30) Shu, T.; Zhou, Z.; Wang, H.; Liu, G.; Xiang, P.; Rong, Y.; H., H.; Zhao, Y. *J. Mater. Chem.* **2012**, *22*, 10525−10529.
(31) Xi, J.; Zhang, Q.; Park, K.; Sun, Y.; Cao, G. *Electrochim. Acta* **2011**, *56*, 1960−1966.
(32) Shen, Q.; Toyoda, T. *Jpn. J. Appl. Phys.* **2004**, *43*, 2946−2951.
(33) Gao, R.; Wang, L.; Geng, Y.; Ma, B.; Zhu, Y.; Dong, H.; Qiu, Y. *Phys. Chem. Chem. Phys.* **2011**, *13*, 10635−10640.
(34) Gao, R.; Wang, L.; Geng, Y.; Ma, B.; Zhu, Y.; Dong, H.; Qiu, Y. *J. Phys. Chem. C* **2011**, *115*, 17986−17992.
(35) Gao, R.; Wang, L.; Ma, B.; Zhan, C.; Qiu, Y. *Langmuir* **2010**, *26*, 2460−2465.
(36) Cao, G.; Wang, Y. *Nanostructures and Nanomaterials*; World Scientifics Publishing Co. Pte. Ltd.: Singapore, 2011.
(37) Koide, N.; Islam, A.; Chiba, Y.; Han, L. Y. *J. Photochem. Photobiol. A-Chem.* **2006**, *182*, 296−305.
(38) Wang, Q.; Ito, S.; Gratzel, M.; Fabregat-Santiago, F.; Mora-Sero, I.; Bisquert, J.; Bessho, T.; Imai, H. *J. Phys. Chem. B* **2006**, *110*, 25210−25221.
(39) Bisquert, J.; Fabregat-Santiago, F.; Mora-Sero, I.; Garcia-Belmonte, G.; Gimenez, S. *J. Phys. Chem. C* **2009**, *113*, 17278−17290.